ENGINEERING Information Technology & Electronic Engineering
https://www.academax.com/EITEE; https://www.engineering.org.cn
https://ieeexplore.ieee.org/xpl/RecentIssue.jsp?punumber=11344065
E-mail: eng.itee@zju.edu.cn

Engineering Journals
Available on IEEE Xplore®

Research Article
https://doi.org/10.1631/ENG.ITEE.2026.0255

Tracking of Target Groups with Time-Varying Shapes Using Multiple Shape Dynamic Models

Jie SHI[1], Xiaomeng CAO[1✉], Weifeng LIU[1], Yuntao LUO[1]

[1]*School of Electrical and Control Engineering, Shaanxi University of Science and Technology, Xi'an, China*

Abstract: In recent years, group target tracking (GTT) has received widespread attention. Due to limited radar resolution, many existing approaches treat a target group as a whole and focus on the estimation of the kinematic state and shape of the target group, without directly considering the individual properties of each target within the group. Most of these approaches assume that the group shape is time-invariant or slowly time-varying. In practice, target groups influenced by task intentions may exhibit behaviors such as expansion and contraction, and their shapes are time-varying. Accurate tracking of target groups with time-varying shapes is challenging using these traditional approaches. To address this challenge, this paper proposes a tracking approach for target groups with time-varying shapes. First, based on a Gaussian process model in which the target group shape is represented by radial distances from the centroid to several boundary points, this paper incorporates radial velocities into the dynamic model of the radial distances. Accordingly, a new shape dynamic model is proposed to characterize the time-varying evolution of the target group shape using radial velocities, such as expansion and contraction. For different shape dynamic models, the corresponding models adopt distinct sets of radial velocities. Based on these shape dynamic models, the target group tracking approach is developed using interacting multiple model (IMM) framework to rapidly identify true evolution modes and match suitable tracking models. Simulation results demonstrate the effectiveness of the proposed approach in terms of tracking accuracy and shape estimation performance.

Key words: Target group tracking; Time-varying shape; Gaussian processes; Interacting multiple models

1 Introduction

With the rapid development of unmanned systems, swarm intelligence, and cooperative sensing technologies, target group tracking has attracted increasing attention in situation awareness applications (Ricardo et al., 2023). In practical scenarios, UAV formations, naval vessel groups, and ground vehicle groups dynamically alter their layouts according to surrounding conditions and movement demands (Yasin et al., 2020; Shi et al., 2022; Zhang et al., 2024). Target groups can expand for broader sensing coverage, contract to traverse narrow spaces, or modify their internal layout in the course of motion. These behaviors result in diverse time-varying shape characteristics of target groups. Due to limited sensor resolution, individual targets within a target group cannot be clearly resolved. Therefore, most existing approaches regard the target group as a whole and jointly estimate its kinematic state and shape from measurements (Mannari et al., 2024; Granstrom et al., 2016). Different spatial distributions of targets within a group may lead to different measurement distributions. Specifically, when targets are distributed along the group boundary, with no targets located in the interior, measurements are generated from the target group contour. In the other case, targets are distributed within the space occupied by the group, and corresponding measurements are uniformly distributed over the group shape. In addition, target group tracking also faces many other challenges, including clutter, missed detections, nonuniform interior measurement density, and uncertain measurement-to-boundary association. A foundation solving these problems lies in accurate target group tracking under ideal conditions, with no clutter and uniformly distributed measurements. Following many other existing works (Koch, 2008; Baum and Hanebeck, 2014; Yang and Baum, 2019), we also focus on solving a fundamental problem of tracking a target group in such conditions.

✉ Xiaomeng CAO, xmcao911@163.com
Jie SHI, https://orcid.org/0009-0002-0369-0003
Xiaomeng CAO, https://orcid.org/0000-0003-4100-7164
Weifeng LIU, https://orcid.org/0000-0001-9537-8767
Yuntao LUO, https://orcid.org/0009-0003-2907-6412
CLC number: TPxxx

Received: Aug. 11, 2026; Revision accepted: Sept. 27, 2026

In recent years, extensive research has focused on shape modeling of extended targets and target groups. Early approaches mainly relied on geometric models, such as circular and elliptical representations (Koch, 2008; Tuncer and Özkan, 2021; Lan and Li, 2012; Tuncer et al., 2022). Random hypersurface models (RHM) further improved the flexibility of shape representation by describing target contours using radial functions (Baum and Hanebeck, 2009; Wang and Zhan, 2024). To handle more complex irregular and nonconvex shapes, level-set methods and Gaussian process(GP) approaches have been developed, providing more flexible representations of target contours (Zea et al., 2016; Wahlström and Özkan, 2015; Yang et al., 2023; Li and Song, 2020). Furthermore, spatio-temporal Gaussian process (STGP) and extension deformation approaches (EDA) have been proposed to model complex shape variations using temporal deformation mechanisms or compact shape parameterizations (Aftab et al., 2019; Cao et al., 2021, 2026). Although these studies have significantly improved the capability of representing complex shapes in extended target and target group tracking, they are typically developed for time-invariant or slowly varying shapes.

Compared with shape representation, the dynamic modeling of time-varying target group shapes remains relatively less studied. Stochastic process modeling and online learning have been investigated to describe temporal evolution in target tracking (Li et al., 2025). Existing studies on the dynamic modeling of extended and group targets mainly focus on state estimation, including PMBM multi-sensor tracking frameworks, graph group tracking methods, and irregular extended target tracking approaches under unknown measurement noise covariance (Xue et al., 2024; Zhang et al., 2023; Xu et al., 2024). However, most existing methods employ a single shape dynamic model and rarely construct multiple shape dynamic models to describe different shape evolution modes. The IMM framework has been widely used in maneuvering target tracking by switching between different kinematic models (Yan et al., 2024; Li et al., 2023), while its application to multiple shape evolution modes of target groups remains limited. Meanwhile, change-detection and sliding-window methods have been developed to handle abrupt shape variations (Lau et al., 2019; Xie et al., 2021; Kang and Baek, 2021). Our previous work addressed abrupt shape changes using Gaussian processes (Shi et al., 2025), but it merely considers shape variations and fails to build multiple shape dynamic models to describe the time-varying evolution of target group shapes.

Motivated by this, this paper addresses the problem of tracking target groups with time-varying shapes. Shape states are represented using radial distance functions from the centroid to boundary points and are modeled in a nonparametric manner via Gaussian processes. To characterize the time-varying evolution of target group shape, radial velocities are incorporated into the dynamic model of the radial distances to construct a shape dynamic model. For different shape evolution modes, multiple shape dynamic models with distinct sets of radial velocities are constructed to describe different evolution behaviors, such as expansion and contraction. Based on these shape dynamic models, the target group tracking approach is developed using an interacting multiple model (IMM) framework to rapidly identify the true evolution modes and match suitable tracking models.

To sum up, this paper makes the primary contributions in the following aspects:

- A new idea is proposed by introducing radial velocities into the dynamic model of radial distances. It can characterize the time-varying evolution of the target group shape.
- Based on this idea, multiple shape dynamic models with distinct sets of radial velocities are constructed. These models can describe different shape evolution modes, such as expansion and contraction.
- Based on these shape dynamic models, a tracking approach for target groups with time-varying shapes is developed by using IMM. This enables rapid identification of the true evolution modes and matching of suitable tracking models.

2 Background Knowledge

2.1 Gaussian Process

In this subsection, a Gaussian process (GP) model is utilized to describe the radial function of a target group. Specifically, the angular direction θ is taken as the GP input, while the corresponding radial distance $r = f(\theta)$ is regarded as the GP output. Accordingly, the target group contour is represented by a radial function over the interval $\theta \in [0, 2\pi)$.

2.1.1 Mean Function

A GP defines a distribution over functions such that any finite set of function values follows a multivariate Gaussian distribution. For a set of angular observations $\boldsymbol{\theta} = [\theta_1, \ldots, \theta_N]^T$, the corresponding radial distances are denoted by $\boldsymbol{f} = [f(\theta_1), \ldots, f(\theta_N)]^T$. In this paper, similar to (Wahlström and Özkan, 2015), the GP is assumed to have a constant mean function:

$$\mu(\theta) = r_0, \quad r_0 \sim \mathcal{N}(0, \sigma_r^2). \tag{1}$$

Accordingly, the radial distance function is modeled as

$$f(\theta) \sim \mathcal{GP}\big(\mu(\theta), K(\theta, \theta')\big), \tag{2}$$

where $\mu(\theta)$ denotes the mean function, and $K(\theta, \theta')$ denotes the covariance function.

2.1.2 Covariance Function

To characterize the periodic property of the target group contour, a periodic kernel function is adopted:

$$K(\theta, \theta') = \sigma_f^2 \exp\left(-\frac{2\sin^2\left(\frac{|\theta-\theta'|}{2}\right)}{d^2}\right) + \sigma_r^2. \tag{3}$$

where σ_f^2 denotes the signal variance, d is the length-scale parameter, and σ_r^2 represents the variance of the mean function.

It can be observed that when $\theta \approx \theta'$ or $\theta \approx \theta' + 2\pi$, the kernel value reaches its maximum, indicating strong correlation between correlated angular directions. This property enables a smooth representation of the target group contour.

2.2 Target Group Shape Dynamic Model

In the GP-based extended target tracking (ETT) framework, the kinematic state and shape state of the target are jointly estimated (Wahlström and Özkan, 2015). In this paper, the unresolved target group is represented as an extended object, and its kinematic state and shape state are estimated simultaneously. Therefore, the state transition equation of the target group at time step k is given by:

$$\boldsymbol{x}_{k+1} = \boldsymbol{F}_k \boldsymbol{x}_k + \boldsymbol{\omega}_k, \tag{4}$$

where $\boldsymbol{x}_k = \left[\bar{\boldsymbol{x}}_k^{\mathrm{T}} \quad (\boldsymbol{x}_k^{\mathrm{f}})^{\mathrm{T}}\right]^{\mathrm{T}}$, denotes the state vector of the target group. Here, $\bar{\boldsymbol{x}}_k = \left[(\boldsymbol{x}_k^{\mathrm{c}})^{\mathrm{T}} \ (\boldsymbol{x}_k^{*})^{\mathrm{T}}\right]^{\mathrm{T}}$ represents the centroid kinematic state, which consists of the centroid position $\boldsymbol{x}_k^{\mathrm{c}}$ and kinematic parameters $\boldsymbol{x}_k^{*}$ (e.g.velocity, acceleration), and $\boldsymbol{x}_k^{\boldsymbol{b}} = \left[f_k(\theta_1^{\boldsymbol{b}}), f_k(\theta_2^{\boldsymbol{b}}), \ldots, f_k(\theta_{N_f}^{\boldsymbol{b}})\right]^{\mathrm{T}}$ is the radial shape state. In this definition, $\boldsymbol{\theta}^{\boldsymbol{b}} = [\theta_1^{\boldsymbol{b}}, \theta_2^{\boldsymbol{b}}, \ldots, \theta_{N_f}^{\boldsymbol{b}}]^T$ represents N_f equidistant angular basis points over the interval $[0, 2\pi)$, and each element of $\boldsymbol{x}_k^{\boldsymbol{b}}$ corresponds to the radial distance from the centroid to the target group contour along the associated angular direction. The state transition matrix is given by $\boldsymbol{F}_k = \mathrm{diag}(\boldsymbol{F}_k^{cv}, \boldsymbol{F}_k^{\boldsymbol{b}})$, where $\boldsymbol{F}_k^{\boldsymbol{b}} = e^{-\alpha T}\boldsymbol{I}$, with α denoting the forgetting factor. The process noise $\boldsymbol{\omega}_k \sim \mathcal{N}(\boldsymbol{0}, \boldsymbol{Q}_k)$ is assumed to be zero-mean Gaussian noise with covariance $\boldsymbol{Q}_k = \mathrm{diag}(\boldsymbol{Q}_k^{cv}, \boldsymbol{Q}_k^{\boldsymbol{b}})$, where $\boldsymbol{Q}_k^{\boldsymbol{b}} = (1 - e^{-2\alpha T})K(\boldsymbol{\theta}^{\boldsymbol{b}}, \boldsymbol{\theta}^{\boldsymbol{b}})$.

2.3 Measurement Model

This paper focuses on target group tracking with time-varying shapes. Two spatial distributions of measurements are considered: measurements generated from the target group contour when targets are distributed along the boundary with no targets located in the interior, and measurements uniformly distributed over the target group shape when targets are distributed within the space occupied by the group. The corresponding measurement models are presented next.

2.3.1 Model for contour measurement

When the measurements are generated from the contour of the target group, the measurement model can be expressed as

$$\boldsymbol{z}_{k,l} = \boldsymbol{x}_k^c + \boldsymbol{p}(\theta_{k,l}) f(\theta_{k,l}) + \bar{\boldsymbol{e}}_{k,l} \tag{5}$$

where $\boldsymbol{x}_k^c$ denotes the centroid position of the target group at time step k, $\boldsymbol{z}_{k,l}$ represents the l-th measurement generated by the target group at time step k, $\theta_{k,l}$ denotes the corresponding measurement direction, $f(\theta_{k,l})$ represents the radial distance along the direction $\theta_{k,l}$, and $\bar{\boldsymbol{e}}_{k,l} \sim \mathcal{N}(\boldsymbol{0}, \boldsymbol{R})$ denotes the measurement noise. The direction vector corresponding to $\theta_{k,l}$ is denoted by

$$\boldsymbol{p}(\theta_{k,l}) = \frac{\boldsymbol{z}_{k,l} - \boldsymbol{x}_k^c}{\|\boldsymbol{z}_{k,l} - \boldsymbol{x}_k^c\|}. \tag{6}$$

2.3.2 Model for interior measurement

When the measurements are generated over the target group shape, the contour measurement model can be extended to the interior measurement model by introducing a scaling factor:

$$\boldsymbol{z}_{k,l} = \boldsymbol{x}_k^c + s_{k,l} \boldsymbol{p}(\theta_{k,l}) f(\theta_{k,l}) + \bar{\boldsymbol{e}}_{k,l}, \tag{7}$$

where $s_{k,l} \in [0,1]$ denotes the scaling factor, when $s_{k,l} = 1$, the model reduces to the target contour measurement model. The radial function can be represented in the GP state-space form as $\boldsymbol{H}^{\boldsymbol{b}}(\theta_{k,l})\boldsymbol{x}_k^{\boldsymbol{b}} + \boldsymbol{e}_{k,l}^{\boldsymbol{b}}$, where $\boldsymbol{H}^{\boldsymbol{b}}(\theta_{k,l})\boldsymbol{x}_k^{\boldsymbol{b}}$ denotes the mean radial distance corresponding to the direction $\theta_{k,l}$, and $\boldsymbol{e}_{k,l}^{\boldsymbol{b}}$ denotes the Gaussian radial noise satisfying $\boldsymbol{e}_{k,l}^{\boldsymbol{b}} \sim \mathcal{N}(\boldsymbol{0}, \boldsymbol{R}_{k,l}^{\boldsymbol{b}})$. Therefore, the measurement equation can be further rewritten as

$$\begin{aligned}
\boldsymbol{z}_{k,l} &= \boldsymbol{x}_k^c + \boldsymbol{p}_{k,l}(\boldsymbol{x}_k^c)\left[\boldsymbol{H}^{\boldsymbol{b}}(\theta_{k,l}(\boldsymbol{x}_k^c))\boldsymbol{x}_k^{\boldsymbol{b}} + \boldsymbol{e}_{k,l}^{\boldsymbol{b}}\right] + \bar{\boldsymbol{e}}_{k,l} \\
&= \underbrace{\boldsymbol{x}_k^c + \widetilde{\boldsymbol{H}}_l(\boldsymbol{x}_k^c)\boldsymbol{x}_k^{\boldsymbol{b}}}_{h_{k,l}(\boldsymbol{x}_k)} + \underbrace{\boldsymbol{p}_{k,l}(\boldsymbol{x}_k^c)\boldsymbol{e}_{k,l}^{\boldsymbol{b}} + \bar{\boldsymbol{e}}_{k,l}}_{\boldsymbol{e}_{k,l}} \\
&= h_{k,l}(\boldsymbol{x}_k) + \boldsymbol{e}_{k,l}, \qquad \boldsymbol{e}_{k,l} \sim \mathcal{N}(\boldsymbol{0}, \boldsymbol{R}_{k,l}).
\end{aligned} \tag{8}$$

where $\boldsymbol{e}_{k,l} \sim \mathcal{N}(\boldsymbol{0}, \boldsymbol{R}_{k,l})$. According to (Wahlström and Özkan, 2015), $h_{k,l}(\boldsymbol{x}_k)$ denotes the measurement function, given by

$$h_{k,l}(\boldsymbol{x}_k) = \boldsymbol{x}_k^c + \tilde{\boldsymbol{H}}_l(\boldsymbol{x}_k^c)\boldsymbol{x}_k^{\boldsymbol{b}}, \tag{9}$$

$$\tilde{\boldsymbol{H}}_l(\boldsymbol{x}_k^c) = \boldsymbol{p}_{k,l}(\boldsymbol{x}_k^c)\boldsymbol{H}^{\boldsymbol{b}}(\theta_{k,l}(\boldsymbol{x}_k^c)). \tag{10}$$

The new measurement noise covariance is given by

$$\boldsymbol{R}_{k,l} = \boldsymbol{p}_{k,l}\boldsymbol{R}_{k,l}^{\boldsymbol{b}}\boldsymbol{p}_{k,l}^T + \boldsymbol{R}, \tag{11}$$

$$\boldsymbol{p}_{k,l} = \boldsymbol{p}_{k,l}(\boldsymbol{x}_k^c), \qquad \boldsymbol{R}_{k,l}^{\boldsymbol{b}} = \boldsymbol{R}^{\boldsymbol{b}}(\theta_{k,l}(\boldsymbol{x}_k^c)). \tag{12}$$

The above measurement model is only applicable when the measurements are generated from the target group contour. When the measurements are generated from the interior region of the target group, the corresponding measurement model can be obtained by scaling the contour model using the scaling factor. Specifically, the scaling factor $s_{k,l}$ follows a uniform distribution:

$$s_{k,l}^2 \sim U[0,1]. \tag{13}$$

The mean and variance of $s_{k,l}$ are given by

$$\mu_s = E(s_{k,l}) = \frac{2}{3}. \tag{14}$$

$$\sigma_s^2 = E(s_{k,l}^2) - E(s_{k,l})^2 = \frac{1}{18}. \tag{15}$$

To satisfy the inference conditions of the Gaussian filter, the scaling factor is approximated by a Gaussian random variable with the same first two moments,

$$s_{k,l} \approx \mathcal{N}(\mu_s, \sigma_s^2). \tag{16}$$

Consequently, the measurement equation of the interior measurement model can be further expressed as

$$\begin{aligned}
\boldsymbol{z}_{k,l} &= \underbrace{\boldsymbol{x}_k^c + \mu_s\tilde{\boldsymbol{H}}_l(\boldsymbol{x}_k^c)\boldsymbol{x}_k^{\boldsymbol{b}}}_{\tilde{h}_{k,l}(\boldsymbol{x}_k)} + \underbrace{(s_{k,l} - \mu_s)\tilde{\boldsymbol{H}}_l(\boldsymbol{x}_k^c)\boldsymbol{x}_k^{\boldsymbol{b}} + \bar{\boldsymbol{e}}_{k,l}}_{\tilde{\boldsymbol{e}}_{k,l}} \\
&= \tilde{h}_{k,l}(\boldsymbol{x}_k) + \tilde{\boldsymbol{e}}_{k,l}.
\end{aligned} \tag{17}$$

$$\tilde{h}_{k,l}(\boldsymbol{x}_k) = \boldsymbol{x}_k^c + \mu_s\tilde{\boldsymbol{H}}_l(\boldsymbol{x}_k^c)\boldsymbol{x}_k^{\boldsymbol{b}}, \tag{18}$$

$$\tilde{\boldsymbol{R}}_{k,l} = \boldsymbol{R}_{k,l} + \sigma_s^2\tilde{\boldsymbol{H}}_{k,l}\boldsymbol{x}_k^{\boldsymbol{b}}(\boldsymbol{x}_k^{\boldsymbol{b}})^T\tilde{\boldsymbol{H}}_{k,l}^T, \tag{19}$$

$$\tilde{\boldsymbol{H}}_{k,l} = \tilde{\boldsymbol{H}}_l(\boldsymbol{x}_k^c), \tag{20}$$

where $\tilde{\boldsymbol{e}}_{k,l} \sim \mathcal{N}(\boldsymbol{0}, \tilde{\boldsymbol{R}}_{k,l})$.

3 Shape Dynamic Model for Target Groups Using Radial Velocities

3.1 Motivation

Existing radial representations can flexibly characterize complex target group shapes using radial distances from the centroid to the group boundary. However, these representations are typically developed for time-invariant or slowly varying shapes and do not explicitly describe the temporal evolution of the target group shape. In practical tracking scenarios, the target group shape may vary continuously due to formation adjustment, cooperative motion, task requirements, or environmental constraints. For example, a UAV swarm may expand to increase surveillance coverage, contract to pass through constrained regions, or deform differently along different directions during formation reconfiguration. These behaviors indicate that the radial distances along different angular directions may exhibit different temporal evolution characteristics.

To characterize such time-varying shape evolution, radial velocities are introduced into the dynamic model of the radial distances. Different from the radial distance, which describes the instantaneous distance from the centroid to the group boundary, the radial velocity describes the variation rate of this distance along the corresponding angular direction. A positive radial velocity indicates outward motion of the boundary point along the radial direction, while a negative radial velocity indicates inward motion. By introducing radial velocities, the temporal evolution of the target group shape can be explicitly characterized. This provides a basis for describing typical shape evolution behaviors, such as expansion, contraction, and different variations along angular directions.

3.2 Shape Dynamic Model Using Radial Velocities

The angular basis directions are denoted by $\theta_s^{\boldsymbol{b}}$, $s = 1, \ldots, N_f$, and the corresponding radial distance at time step k is denoted by $f_k(\theta_s^{\boldsymbol{b}})$. The radial velocity along this direction is represented by $v_k(\theta_s^{\boldsymbol{b}})$, which characterizes the variation rate of the radial distance. In this work, the radial velocities are preset as fixed model inputs to describe different shape evolution behaviors. As illustrated in Fig. 1, the radial velocity describes the dynamic variation of the target group shape between time step k and $k+1$ along each angular basis direction.

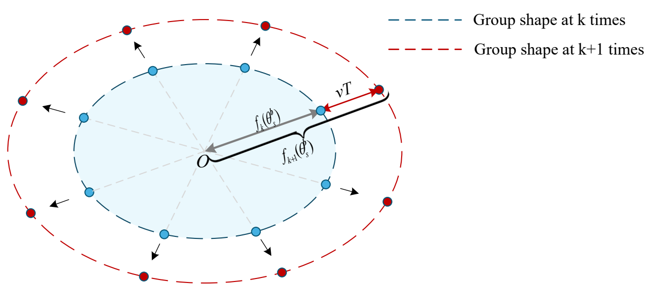

Fig. 1 Schematic of target group shape variation between time step k and $k+1$ described by radial velocity

For a basis point corresponding to the sth angular basis direction, the radial distance dynamic model can be formulated as

$$f_{k+1}(\theta_s^{\boldsymbol{b}}) = e^{-\alpha T} f_k(\theta_s^{\boldsymbol{b}}) + T v_k(\theta_s^{\boldsymbol{b}}) + \omega_k(\theta_s^{\boldsymbol{b}}). \tag{21}$$

where T is the sampling interval, α is the forgetting factor, and $\omega_k(\theta_s^{\boldsymbol{b}})$ denotes the process noise. The corresponding process noise variance along the sth angular basis direction is given by

$$Q_k(\theta_s^{\boldsymbol{b}}) = \left(1 - e^{-2\alpha T}\right) K(\theta_s^{\boldsymbol{b}}, \theta_s^{\boldsymbol{b}}). \tag{22}$$

where $K(\cdot,\cdot)$ is the GP kernel evaluated at the angular basis direction.

This idea provides a simple and intuitive way to describe the dynamic variation of target group shape. By introducing radial velocities, the time-varying evolution of the target group shape can be explicitly characterized.

Remark 1: By assigning radial velocities to different angular directions, the proposed model can describe shape variations with different evolution rates. Compared with conventional models that rely only on radial distance evolution, the proposed formulation provides a more flexible representation of time-varying shape changes. This enables the model to describe practical target group behaviors, such as expansion, contraction, and shape variations along different directions. As a result, the proposed model enables better accommodation of shape variations and facilitates more accurate shape estimation and better target group tracking performance.

3.3 Overall Dynamic Model

Based on the radial distance dynamic model described above, radial velocities along all angular basis directions are incorporated to characterize the overall evolution of the target group shape. Accordingly, the state vector of the target group at time step k is defined as:

$$\boldsymbol{x}_k = \left[\bar{\boldsymbol{x}}_k^{\mathrm{T}}, (\boldsymbol{x}_k^{\boldsymbol{b}})^{\mathrm{T}}\right]^{\mathrm{T}}, \tag{23}$$

$$\bar{\boldsymbol{x}}_k = \left[(\boldsymbol{x}_k^{\mathrm{c}})^{\mathrm{T}}, (\boldsymbol{x}_k^{*})^{\mathrm{T}}\right]^{\mathrm{T}}, \tag{24}$$

where $\boldsymbol{x}_k^{\mathrm{c}}$ and $\boldsymbol{x}_k^{*}$ denote the centroid position and velocity of the target group, respectively. The radial shape state is expressed as $\boldsymbol{x}_k^{\boldsymbol{b}} = \left[f_k(\theta_1^{\boldsymbol{b}}), f_k(\theta_2^{\boldsymbol{b}}), \ldots, f_k(\theta_{N_f}^{\boldsymbol{b}})\right]^{\mathrm{T}}$.

By incorporating the radial velocity terms into the state transition model in (4), the state transition process of the target group is reformulated as

$$\boldsymbol{x}_{k+1} = \boldsymbol{F}_k \boldsymbol{x}_k + \boldsymbol{B} T \boldsymbol{v}_k^{\boldsymbol{b}} + \boldsymbol{\omega}_k, \tag{25}$$

$$x_0 \sim \mathcal{N}(\boldsymbol{\mu}_0, P_0), \tag{26}$$

where $\boldsymbol{F}_k$ denotes the state transition matrix, and $\boldsymbol{\omega}_k$ represents the process noise following a Gaussian distribution with zero mean and covariance $\boldsymbol{Q}_k$, formulated as:

$$\boldsymbol{F}_k = \begin{bmatrix} \boldsymbol{F}_k^{cv} & \boldsymbol{0} \\ \boldsymbol{0} & \boldsymbol{F}_k^{\boldsymbol{b}} \end{bmatrix}, \qquad \boldsymbol{B} = \begin{bmatrix} \boldsymbol{0}_{4\times N_f} \\ \boldsymbol{I}_{N_f} \end{bmatrix}, \tag{27}$$

$$\boldsymbol{\mu}_0 = \begin{bmatrix} \bar{\boldsymbol{\mu}}_0 \\ \boldsymbol{0} \end{bmatrix}, \qquad \boldsymbol{P}_0 = \begin{bmatrix} \bar{\boldsymbol{P}}_0 & \boldsymbol{0} \\ \boldsymbol{0} & \boldsymbol{P}_0^{\boldsymbol{b}} \end{bmatrix}, \tag{28}$$

$$\boldsymbol{F}_k^{\boldsymbol{b}} = e^{-\alpha T} \boldsymbol{I}_{N_f}, \boldsymbol{Q}_k = \mathrm{diag}\left(\boldsymbol{Q}_k^{cv}, \boldsymbol{Q}_k^{\boldsymbol{b}}\right), \tag{29}$$

$$\boldsymbol{Q}_k^{\boldsymbol{b}} = \left(1 - e^{-2\alpha T}\right) K\left(\boldsymbol{\theta}^{\boldsymbol{b}}, \boldsymbol{\theta}^{\boldsymbol{b}}\right), \tag{30}$$

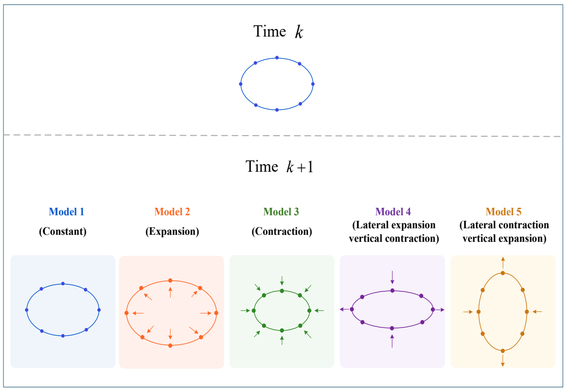

Fig. 2 Illustration of target group shape dynamic models

$$\boldsymbol{v}_k^{\boldsymbol{b}} = \left[v_k(\theta_1^{\boldsymbol{b}}), v_k(\theta_2^{\boldsymbol{b}}), \ldots, v_k(\theta_{N_f}^{\boldsymbol{b}}) \right]^{\mathrm{T}}. \tag{31}$$

where T denotes the sampling period and α represents the forgetting factor. Together with the measurement model established in Section 2.3, the proposed formulation enables dynamic modeling of target groups with time-varying shapes.

4 Multi-Model Tracking for Target Groups with Time-Varying Shapes

4.1 Motivation

In practical target group tracking scenarios, target groups may exhibit different shape evolution behaviors due to task requirements, formation adjustments, or environmental constraints. For example, a target group may maintain its original formation, undergo overall expansion or contraction, or experience shape variations along different directions during formation adjustments. These different evolution behaviors lead to distinct shape variation modes over time.

When all boundary points evolve with the same radial velocity, the target group undergoes uniform expansion or contraction while maintaining its overall shape. In more complex scenarios, radial velocities may vary across angular directions, resulting in different shape variations along different directions. Since these shape evolution patterns have different dynamic characteristics, a single fixed model may not be sufficient to describe the various shape evolution behaviors of target groups. Therefore, to improve the adaptability to different shape evolution behaviors, multiple shape dynamic models are constructed within an interacting multiple model (IMM) framework in this subsection.

4.2 Multiple Shape Dynamic Models

Based on the radial velocity-based shape dynamic model established in Section 3, different shape evolution behaviors can be characterized by assigning different radial velocity vectors to the input $\boldsymbol{v}_k^{\boldsymbol{b}}$. As illustrated in Fig. 2, the target group shape at time k may evolve into different shapes at time $k+1$ under different sets of radial velocities. When all boundary points have the same radial velocity, the target group undergoes uniform expansion or contraction, with the radial distances along different angular directions changing at the same rate. In more complex cases, the radial velocities vary across angular directions, resulting in direction-dependent shape variations. To characterize these representative shape evolution behaviors, five shape dynamic models are constructed. These models form the shape dynamic model set defined as

$$\boldsymbol{M} = \{M_1, M_2, M_3, M_4, M_5\}. \tag{32}$$

Each model corresponds to a typical target group shape evolution pattern and will be introduced in detail as follows.

Model 1 (Constant):

This model represents the case where the target group shape remains unchanged. Therefore, the radial velocity of all boundary points is set to zero:

$$v_k(\theta_s^{\boldsymbol{b}}) = 0. \tag{33}$$

Model 2 (Expansion):

A uniform expansion mode is considered by assigning the same positive radial velocity to all angular directions. In this case, all boundary points move outward at the same rate, and the radial velocity is given by

$$v_k(\theta_s^{\boldsymbol{b}}) = v_1, \tag{34}$$

where $v_1 > 0$ denotes the expansion velocity magnitude. This velocity magnitude and those introduced below can be designed a priori.

Model 3 (Contraction):

The contraction mode is obtained by reversing the direction of the radial velocity in Model 2. Specifically, all boundary points move inward with the same velocity magnitude:

$$v_k(\theta_s^{\boldsymbol{b}}) = -v_2, \tag{35}$$

where $v_2 > 0$ denotes the contraction velocity magnitude.

Model 4 (Lateral Expansion with Vertical Contraction):

To describe shape variations along different directions, the radial velocity is allowed to change with the angular direction. In this mode, the target group expands laterally and contracts vertically. The radial velocity is defined as

$$v_k(\theta_s^{\boldsymbol{b}}) = v_3 \Delta\varepsilon, \tag{36}$$

where $v_3 > 0$ denotes the velocity magnitude and $\Delta\varepsilon = \cos(2\theta_s^{\boldsymbol{b}})$ is the modulation factor controlling the directional variation of the radial velocity.

Model 5 (Lateral Contraction with Vertical Expansion):

The opposite directional variation of Model 4 is represented by changing the sign of the modulation factor. The resulting radial velocity is expressed as

$$v_k(\theta_s^{\boldsymbol{b}}) = -v_4 \Delta\varepsilon, \tag{37}$$

where $v_4 > 0$ denotes the velocity magnitude. This setting causes inward motion in the lateral direction and outward motion in the vertical direction.

These models are incorporated into the subsequent multiple-model tracking framework.

Remark 2: Since the radial velocity pattern space is continuous, different radial velocity patterns can be selected to construct candidate shape evolution models. Each model corresponds to a specific radial velocity pattern and characterizes a representative target group shape evolution behavior. It is generally believed that a larger number of models in $\boldsymbol{M}$ leads to more accurate estimation results in the tracking framework. However, using too many sampled models may instead degrade estimation performance (Li and Bar-Shalom, 1996). A possible solution to this problem is to adopt variable-structure multiple-model (VSMM) approaches (Li and Bar-Shalom, 1996; Rong Li and Jilkov, 2005; Lan et al., 2011). Specifically, VSMM approaches, e.g., the best model augmentation (BMA) approach which uses the Kullback-Leiber (KL) criterion to adapt the model set online, can be utilized in our approach for online model-set updating (Lan et al., 2011). For our approach, by treating the radial-velocity magnitude as an adjustable input parameter in the shape dynamic model, the optimal model along with its magnitude can be obtained by using the minimum-KL criterion in BMA, as in (Wei et al., 2025). Then the obtained optimal model can be incorporated into the basic models to construct the candidate shape-model set. We will consider this in future work.

4.3 Filtering Estimation

A hybrid system framework is adopted to model target groups with time-varying shapes. In a hybrid system, a mathematical model set $\boldsymbol{M}$ is used to match the actual shape evolution modes for state estimation. Based on the models in $\boldsymbol{M}$, state estimates are obtained by the corresponding filters, and the final state estimate is obtained by fusing the estimates from different models. For the target group tracking problem with time-varying shapes, the following hybrid system is constructed:

$$\boldsymbol{x}_{k+1}^i = \boldsymbol{F}_k \boldsymbol{x}_k^i + \boldsymbol{B} T \boldsymbol{v}_k^{\boldsymbol{b},i} + \boldsymbol{\omega}_k^i. \tag{38}$$

$$\boldsymbol{z}_{k,l} = h_{k,l}(\boldsymbol{x}_k^i) + \boldsymbol{e}_{k,l}^i. \tag{39}$$

where $i \in \{1, \ldots, \tilde{M}\}$ denotes the index of the shape evolution model, $\boldsymbol{x}_k^i$ is the state vector under model i, $\boldsymbol{v}_k^{\boldsymbol{b},i}$ represents the radial velocity vector corresponding to the shape dynamic model, $\boldsymbol{\omega}_k^i$ is the process noise, $\boldsymbol{h}_{k,l}(\cdot)$ denotes the nonlinear measurement function for the l-th measurement. In the sequel, $m_k^{(i)}$ denotes model i or the event that the target group evolves according to model i at time k.

The model set has been constructed in Section 4.2, which contains five shape dynamic models. In practice, changes in the overall shape of the target group may result in switching among different shape dynamic models. In this case, the model sequence $\langle m_k^{(i)} \rangle$ is usually assumed to be a first-order homogeneous Markov chain with transition probabilities (Li and Bar-Shalom, 1996; Rong Li and Jilkov, 2005).

$$\pi_{ij} = P\left(m_{k+1}^{(j)} \mid m_k^{(i)}\right), \qquad i,j = 1, \ldots, \tilde{M}. \tag{40}$$

One cycle of the proposed IMM filtering procedure consists of the following steps.

1) Mixing probability computation. The probability that model $m_k^{(i)}$ was in effect at time k, given that model $m_{k+1}^{(j)}$ is in effect conditioned on $\boldsymbol{Z}^k$, is denoted by $\mu_k^{(i|j)}$. It is calculated using the transition probability π_{ij} and the model probability $P\{m_k^{(i)}|\boldsymbol{Z}^k\}$, according to (Rong Li and Jilkov, 2005), where $i,j = 1, \ldots, \tilde{M}$.

2) State reinitialization. Starting with $\hat{\boldsymbol{x}}_{k|k}^{(i)}$, $\boldsymbol{P}_{k|k}^{(i)}$, and $\mu_k^{(i|j)}$, the mixed initial state $\hat{\boldsymbol{x}}_{k|k}^{(0j)}$ and covariance $\boldsymbol{P}_{k|k}^{(0j)}$ are computed for the filter matched to model $m_{k+1}^{(j)}$.

3) Model-conditioned filtering. The mixed initial state $\hat{\boldsymbol{x}}_{k|k}^{(0j)}$ and covariance $\boldsymbol{P}_{k|k}^{(0j)}$ are used as inputs to the EKF under model $m_{k+1}^{(j)}$, yielding the model-conditioned state estimate $\hat{\boldsymbol{x}}_{k+1|k+1}^{(j)}$ and covariance $\boldsymbol{P}_{k+1|k+1}^{(j)}$. For each model, the corresponding radial velocity vector $\boldsymbol{v}_k^{\boldsymbol{b},j}$ is incorporated into the shape dynamic model through the input term.

4) Model probability update. The model probability $\mu_{k+1}^{(j)} = P\{m_{k+1}^{(j)}|\boldsymbol{Z}^{k+1}\}$ is obtained from the likelihood function corresponding to the filter under model $m_{k+1}^{(j)}$:

$$\Lambda_{k+1}^{(j)} = p\left(\boldsymbol{Z}_{k+1} \mid m_{k+1}^{(j)}, \boldsymbol{Z}^k\right) = \mathcal{N}\left(\boldsymbol{Z}_{k+1}; \hat{\boldsymbol{Z}}_{k+1|k}^{(j)}, \boldsymbol{S}_{k+1}^{(j)}\right), \tag{41}$$

where $\hat{\boldsymbol{Z}}_{k+1|k}^{(j)}$ is the predicted measurement under model $m_{k+1}^{(j)}$, and $\boldsymbol{S}_{k+1}^{(j)}$ is the corresponding innovation covariance.

5) Estimate fusion. The overall state estimate $\hat{\boldsymbol{x}}_{k+1|k+1}$ and covariance $\boldsymbol{P}_{k+1|k+1}$ are obtained from the model-conditioned estimates $\hat{\boldsymbol{x}}_{k+1|k+1}^{(j)}$ and $\boldsymbol{P}_{k+1|k+1}^{(j)}$.

Through the above steps, the proposed IMM framework identifies and probabilistically fuses different shape evolution models based on radial velocities to track target groups with time-varying shapes.

5 Experimental Results

To illustrate the effectiveness of the proposed approach, two simulations are provided in this section.

5.1 Tracking Performance Evaluation for Contour Measurement Scenarios

5.1.1 Scenario Setup

In Scenario 1 (S1), a target group consisting of 15 individual targets is considered. These targets are uniformly distributed along the contour of an ellipse. The initial shape of the group is an ellipse with a major axis of 7 m and a minor axis of 5 m, as depicted in Fig. 3a. The center of the target group starts from [0,0] m and moves according to a constant velocity model with a velocity of [0.3,0.3] m/s, and its trajectory is shown in Fig. 3b. During the 400 s simulation, the target group evolves through a sequence of distinct shape modes. At each discrete time step k, the elliptical group is characterized by its major-axis length A_k and minor-axis length B_k, with corresponding rates of change denoted by v_A and v_B, respectively. The complete mode sequence, along with the prescribed values of v_A and v_B, is detailed in Table 1.

In this scenario, the target group center follows a constant velocity (CV) model, with the model and parameter values given as follows:

$$\boldsymbol{x}_{k+1} = \boldsymbol{F}_k \boldsymbol{x}_k + \boldsymbol{B} T \boldsymbol{v}_k^{\boldsymbol{b}} + \boldsymbol{\omega}_k, \boldsymbol{\omega}_k \sim \mathcal{N}(\boldsymbol{0}, \boldsymbol{Q}_k)$$

$$\boldsymbol{F}_k = \operatorname{diag}\left\{\boldsymbol{F}_k^{cv}, \boldsymbol{F}_k^{\boldsymbol{b}}\right\}, \boldsymbol{Q}_k = \operatorname{diag}\left\{\boldsymbol{Q}_k^{cv}, \boldsymbol{Q}_k^{\boldsymbol{b}}\right\}$$

$$\boldsymbol{F}_k^{cv} = \begin{bmatrix} 1 & T \\ 0 & 1 \end{bmatrix} \otimes \boldsymbol{I}_2, \qquad \boldsymbol{F}_k^{\boldsymbol{b}} = e^{-\alpha T} \boldsymbol{I}_{N_f}$$

Table 1 Evolution modes of the target group

Time (s)	Mode	v_A (m/s)	v_B (m/s)
0–100	M_1	0	0
100–130	M_2	0.20	0.20
130–160	M_3	−0.25	−0.25
160–180	M_2	0.20	0.20
180–260	M_1	0	0
260–300	M_5	−0.10	0.10
300–340	M_4	0.15	−0.15
340–400	M_1	0	0

$$\boldsymbol{B}=\begin{bmatrix}\boldsymbol{0}_{4\times N_f}\\ \boldsymbol{I}_{N_f}\end{bmatrix}, \boldsymbol{Q}_k^{cv}=\begin{bmatrix}\frac{T^3}{3} & \frac{T^2}{2}\\ \frac{T^2}{2} & T\end{bmatrix}\otimes\begin{bmatrix}\sigma_q^2 & 0\\ 0 & \sigma_q^2\end{bmatrix}$$

$$\boldsymbol{Q}_k^{\boldsymbol{b}}=\left(1-e^{-2\alpha T}\right)K(\boldsymbol{\theta^b},\boldsymbol{\theta^b})$$

where $\sigma_q = 0.01$ denotes the process noise standard deviation (Wahlström and Özkan, 2015). A sampling interval of $T = 1$ s and a forgetting factor of $\alpha = 0.0001$ are used. The number of angular basis points for representing the target group shape is set to $N_f = 40$. The radial velocity parameters of the five shape dynamic models are designed a priori and preset as fixed model inputs. Specifically, the radial velocity of Model 1 is set to zero. The radial velocity parameters of Models 2 and 3 are set to $v_1 = 0.10$ m/s and $v_2 = 0.12$ m/s. For Models 4 and 5, the corresponding radial velocity parameters are set to $v_3 = 0.08$ m/s and $v_4 = 0.05$ m/s, respectively.

Generally, the number of received measurements depends on the size of the target group, the distance between the target group and the sensor, and the sensor resolution. In this simulation, for the measurements $\boldsymbol{z}_{k,l}$, all measurements are generated from the target group contour, as shown in Fig. 3c. The number of measurements at each time step follows a Gaussian distribution with a mean of $\lambda = 12$, and the sampled value is rounded to an integer. The measurement model and related parameters are given as follows:

$$\boldsymbol{z}_{k,l}=\boldsymbol{h}_{k,l}(\boldsymbol{x}_k)+\boldsymbol{e}_{k,l}, \boldsymbol{e}_{k,l}\sim\mathcal{N}(\boldsymbol{0},\boldsymbol{R}_{k,l}),$$

The simulation is conducted under a measurement noise covariance of $\boldsymbol{R_{k,l}} = 0.1^2\boldsymbol{I}_2$. The Gaussian process hyperparameters of the proposed method are set to $\sigma_r = 0.5$, $\sigma_f = 1.5$, and $d = \pi/6$. For the sliding-window method, the window length is chosen as $H = 4$, and the change-detection threshold is set to $\tau = 0.8$. The initial model probabilities are uniformly initialized as $\mu_0 = [0.2, 0.2, 0.2, 0.2, 0.2]^T$. Following related IMM-based studies (Eltoukhy et al., 2020; Qian et al., 2024; Han et al., 2019), the self-transition probability is set to 0.96, and the remaining probability is uniformly assigned to the other models. Accordingly, the transition probability matrix is given by

$$\pi_{ij}=\begin{bmatrix}0.96 & 0.01 & 0.01 & 0.01 & 0.01\\ 0.01 & 0.96 & 0.01 & 0.01 & 0.01\\ 0.01 & 0.01 & 0.96 & 0.01 & 0.01\\ 0.01 & 0.01 & 0.01 & 0.96 & 0.01\\ 0.01 & 0.01 & 0.01 & 0.01 & 0.96\end{bmatrix}$$

5.1.2 Compared Algorithms

- GP-EKF : Gaussian process based extended target tracking approach proposed in (Wahlström and Özkan, 2015).
- GP-MMDS : The approach proposed in this paper.
- GP-SW : Following the approach in (Shi et al., 2025), a shape abrupt change detection mechanism based on a sliding window and the Hausdorff distance is adopted as a comparison method. Once an abrupt change is detected, the state vector and covariance matrix are reconstructed from the measurements and then updated recursively using the extended Kalman filter.
- RHM-UKF : The RHM-UKF approach (Baum and Hanebeck, 2014).
- RM : The RM approach (Yang and Baum, 2019).

5.1.3 Evaluation Metrics

To evaluate both centroid tracking accuracy and group shape estimation accuracy, two metrics are adopted: position RMSE and intersection over union (IoU). The position RMSE is used to quantify the centroid estimation error. Let $\boldsymbol{x}_k^c$ denote the true group centroid at time k, and let $\hat{\boldsymbol{x}}_{k,i}^c$ denote the estimated centroid in the i Monte Carlo run. After N Monte Carlo runs, the position RMSE at time k is defined as

$$\mathrm{RMSE}(k)=\sqrt{\frac{1}{N}\sum_{i=1}^{N}\left\|\hat{\boldsymbol{x}}_{k,i}^c-\boldsymbol{x}_k^c\right\|_2^2}. \tag{42}$$

IoU is used to evaluate the overlap between the estimated and target group shapes. Let X_k and $\hat{X}_k$ denote the true and estimated target group regions at time k, respectively. The IoU is defined as

$$\mathrm{IoU}(X_k,\hat{X}_k)=\frac{\mathrm{area}(X_k\cap\hat{X}_k)}{\mathrm{area}(X_k\cup\hat{X}_k)}. \tag{43}$$

where area(·) denotes the area operator. The IoU value lies in the interval $[0, 1]$. A larger IoU indicates better shape estimation accuracy. In particular, IoU = 1 means that the estimated shape perfectly matches the true shape, whereas IoU = 0 means that there is no overlap between them.

5.1.4 Simulation Results

The tracking results averaged over 100 Monte-Carlo simulations are shown in Fig. 3. Compared with GP-EKF, GP-SW, RHM-UKF, and RM method, the proposed method GP-MMDS achieves more accurate shape estimation results. Particularly when different shape evolution modes change, GP-MMDS maintains higher contour estimation accuracy, demonstrating that the constructed multiple shape dynamic models can effectively characterize the time-varying shape evolution of the target group.

The shape estimation results at selected time steps with an interval of 25s are presented in Figs. 3d and 3e. Specifically, the results under Models M1–M3 are presented in Fig. 3d, while those under Models M4 and M5 are presented in Fig. 3e. The estimated contours obtained by GP-MMDS remain close to the true target group shape during different shape evolution processes, especially when the shape evolution mode varies. To quantitatively evaluate the tracking performance, the position RMSE and IoU curves are presented in Figs. 3g and

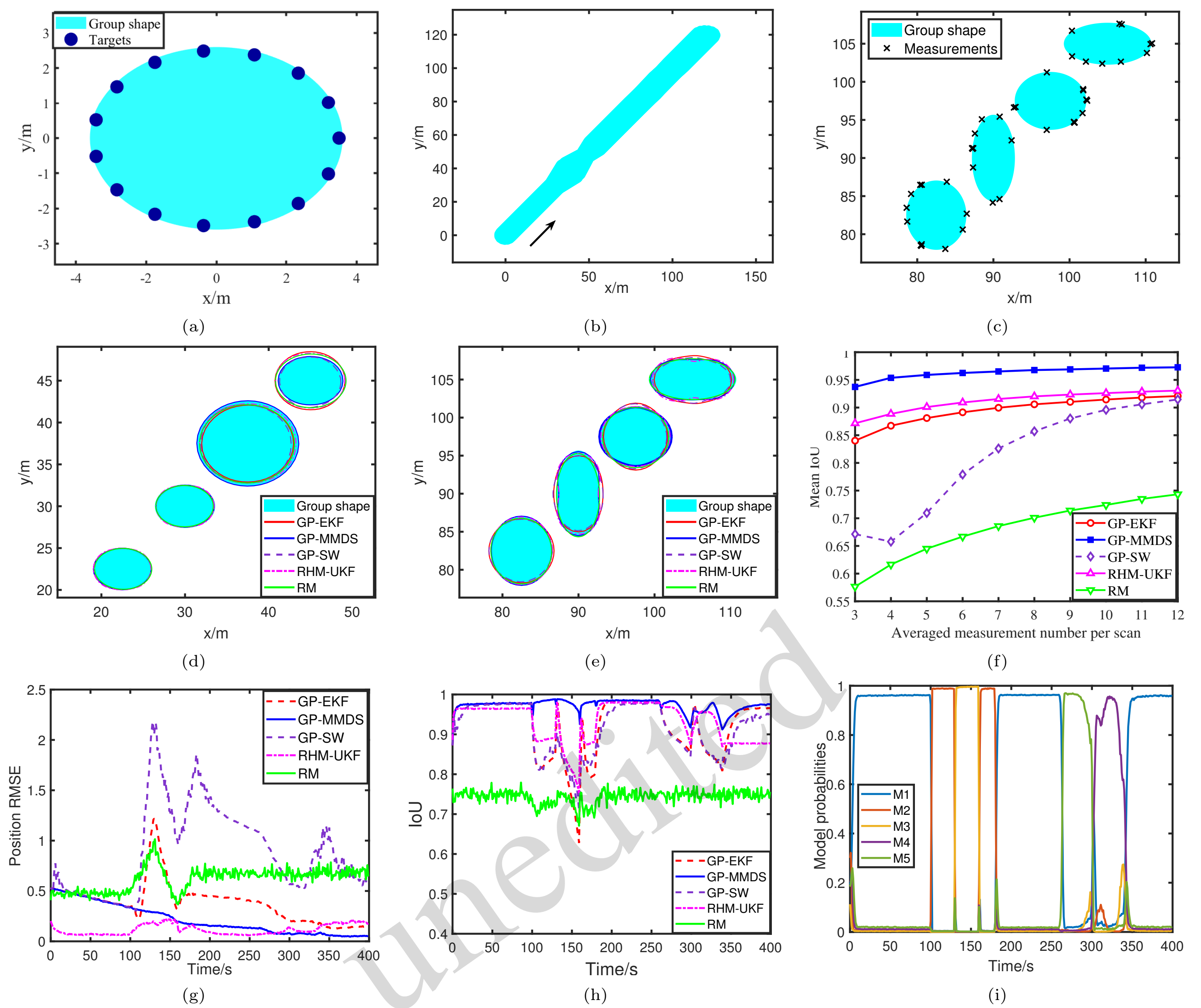

Fig. 3 Estimation results of the compared methods in S1 (averaged over 100 Monte Carlo runs): ***target group consisting of 15 targets and its shape*** **(a),** ***trajectory of the target group*** **(b),** ***measurements*** **(c),** ***estimation results under M1–M3*** **(d),** ***estimation results under M4 and M5*** **(e),** ***mean IoU for different average numbers of measurements per scan*** **(f),** ***position RMSE*** **(g),** ***IoU*** **(h), and** ***model probabilities*** **(i)**

3h, respectively. GP-MMDS maintains a low and stable position RMSE throughout the tracking process while achieving higher IoU values. In particular, when the target group exhibits rapid shape variations, the proposed method maintains better tracking performance. This can be explained by the model probabilities shown in Fig. 3i. The model probability corresponding to the actual shape evolution mode tends to be higher, allowing the IMM framework to assign larger weights to more suitable shape dynamic models during the tracking process.

Furthermore, the influence of the average number of measurements per scan on shape estimation performance is evaluated in Fig. 3f. Overall, the mean IoU rises with more measurements, as extra observations supply more details of the target groups contour. The proposed GP-MMDS always yields the highest average IoU, which verifies its stable performance under different quantities of measurements.

5.2 Tracking Performance Evaluation for Interior Measurement Scenarios

5.2.1 Scenario Setup

In Scenario 2 (S2), the effectiveness of the proposed approach is evaluated in the interior measurement scenario. The same motion model and shape evolution process as those in S1 are adopted, and the resulting target group trajectory is presented in Fig. 4b. Different from S1, the initial shape of the target group is set as a square with a side length of 6 m, and the target group composition is shown in Fig. 4a. The measurements are generated uniformly within the interior of the target group shape, as shown in Fig. 4c. To define its shape evolution consistently with S1, the horizontal and vertical side lengths of the square are regarded as the counterparts of the major-axis length A_k and the minor-axis length B_k of the ellipse, respectively. The number of measurements at each

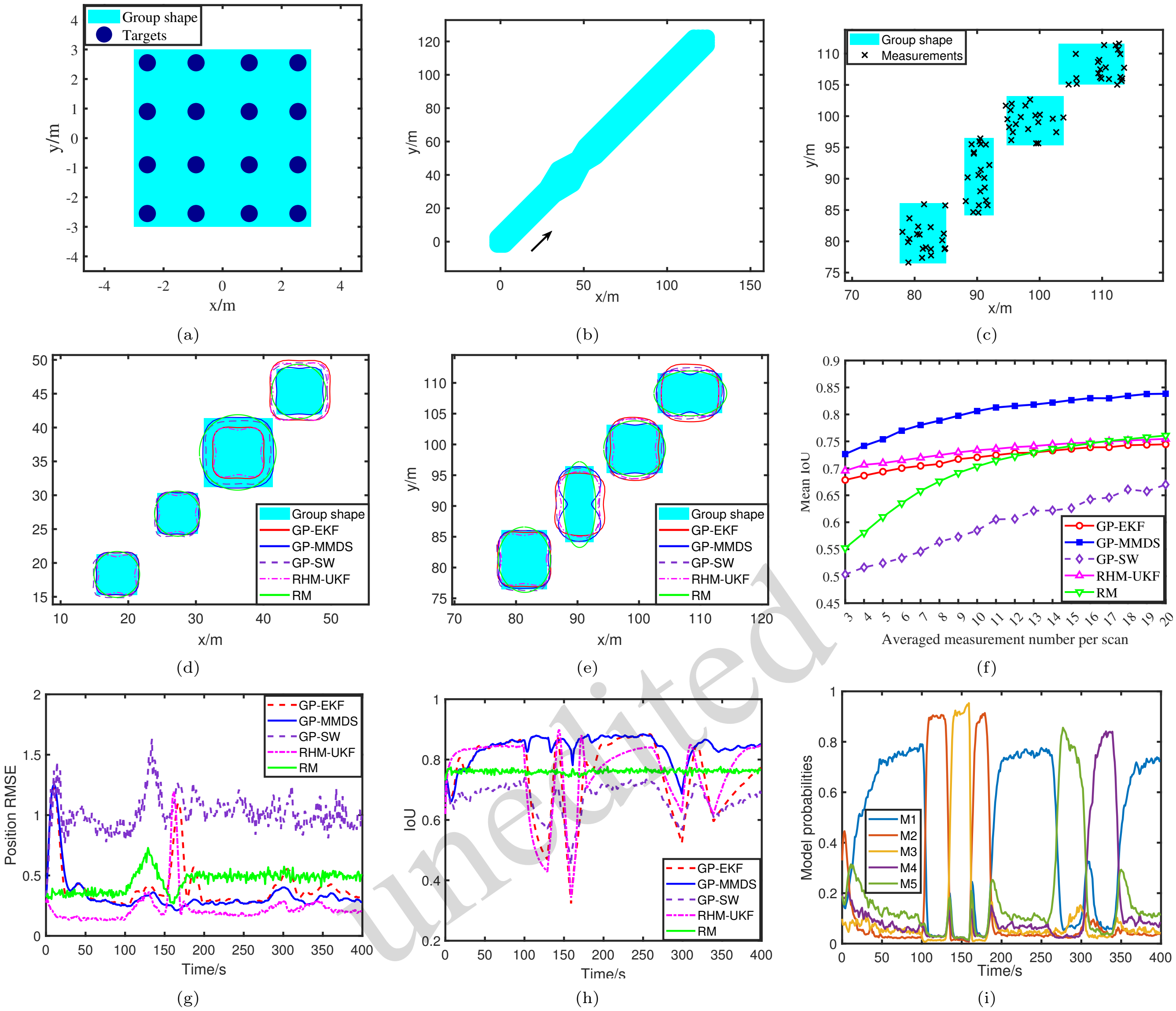

Fig. 4 Estimation results of the compared methods in S2 (averaged over 100 Monte Carlo runs):*target group consisting of 16 targets and its shape* (a), *trajectory of the target group* (b), *measurements* (c), *estimation results under M1–M3* (d), *estimation results under M4 and M5* (e), *mean IoU for different average numbers of measurements per scan* (f), *position RMSE* (g), *IoU* (h), and *model probabilities* (i)

time step follows a Gaussian distribution with a mean value of $\lambda = 20$, and the sampled value is rounded to an integer. Except for the above-mentioned settings, all other parameters are the same as those in S1.

5.2.2 Compared Algorithms

The compared algorithms are the same as those in S1.

5.2.3 Evaluation Metrics

The evaluation metrics are the same as those in S1.

5.2.4 Simulation Results

Figs. 4 and 4i show the simulation results. The shape estimation results at selected time steps with an interval of 30s are presented in Figs. 4d and 4e. Specifically, Fig. 4d shows the estimation results under Models M1–M3, while Fig. 4e presents the results under Models M4 and M5. It can be observed that the contours estimated by GP-MMDS remain close to the true target group shapes during different shape evolution processes. Similar shape estimation performance is also maintained in the interior measurement scenario.

From Fig. 4g, we can see that GP-MMDS maintains relatively stable RMSE performance when the target group undergoes shape changes. This shows that the proposed method can effectively handle the influence of time-varying shape evolution on the tracking process. The IoU results for shape estimation are given in Fig. 4h. Under steady-state conditions, GP-EKF, RHM-UKF, and GP-MMDS all achieve good IoU performance. Although RM gives relatively stable tracking results, its IoU

Table 2 Average runtime per scan of the compared methods (averaged over 100 Monte Carlo runs)

	Method				
Scenario	GP-MMDS	GP-EKF	GP-SW	RHM-UKF	RM
S1 (ms)	2.76	0.64	0.61	4.64	0.18
S2 (ms)	4.14	0.90	0.88	10.82	0.18

values are lower than those of the other methods, indicating that its shape estimation accuracy is limited. GP-SW works well when measurements are mainly distributed near the target group contour, but its estimation accuracy drops in the interior measurement case. Fig. 4i presents model probabilities during shape evolution. The IMM framework quickly identifies the true evolution mode to match suitable tracking models for accurate shape estimation. Thus, GP-MMDS achieves higher IoU when shapes change, showing its validity under interior measurements.

Furthermore, the influence of varying average measurement numbers per scan is investigated in Fig. 4f. It can be observed that the mean IoU values of all methods increase with the number of measurements. Meanwhile, GP-MMDS consistently achieves the highest IoU values across different measurement conditions, demonstrating its robustness to variations in measurement density.

We have added experiments in the interior measurement scenario to evaluate the robustness of GP-MMDS, to variations in the preset radial-velocity magnitudes and the IMM transition probability. The results are shown in Fig. 5. GP-MMDS maintains stable shape estimation performance in both cases, although model mismatch occurs in the former, demonstrating the robustness of the proposed method to parameter variations.

Table 2 shows that RHM-UKF has the longest average runtime, and the average runtime of GP-MMDS is longer than those of GP-EKF, GP-SW, and RM. This is mainly because the proposed multiple-model approach executes five model-conditioned filters in parallel at each scan.

6 Conclusion

For tracking target groups with time-varying shapes, this paper proposes a Gaussian process-based shape dynamic model by introducing radial velocities into the radial distance dynamics. Based on this model, multiple shape dynamic models with different sets of radial velocities are constructed to describe different shape evolution modes. These models are further combined with the IMM framework to identify the current evolution mode and match suitable tracking models.

Simulation results under both contour and interior measurement scenarios demonstrate the effectiveness of the proposed modeling and tracking approach. Future work will extend the proposed approach to more complex conditions involving clutter, detection uncertainty, nonuniform measurement density, and distributed multi-sensor tracking.

Acknowledgments

This work was supported by the National Natural Science Foundation of China (62673307, 62376147) and the Young Talent Fund of Association for Science and Technology in Shaanxi, China (20240126).

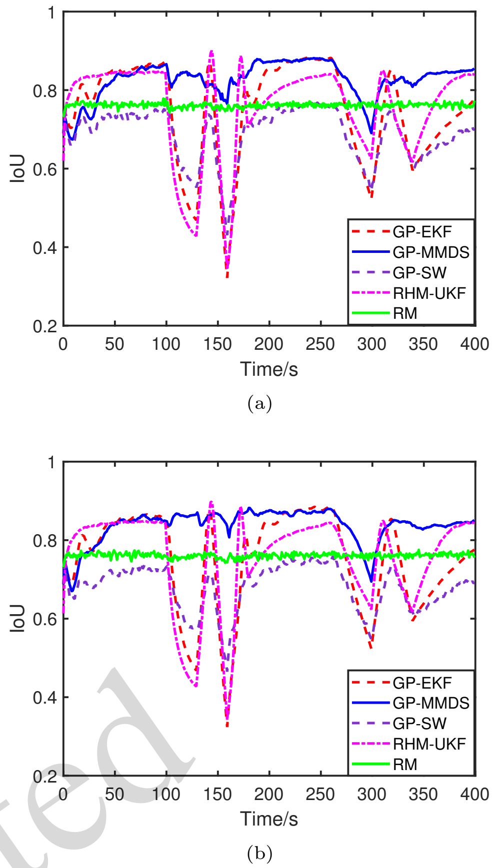

Fig. 5 IoU of GP-MMDS in S2 with *preset radial-velocity magnitudes increased to three times their original values* (a) and *IMM self-transition probability reduced from 0.96 to 0.9* (b)

Author contributions

Jie SHI and Xiaomeng CAO designed the research. Jie SHI and Xiaomeng CAO processed the data. Jie SHI drafted the paper. Weifeng LIU and Yuntao LUO helped organize the paper. Jie SHI, Xiaomeng CAO and Weifeng LIU revised and finalized the paper.

Conflict of interest

All the authors declare that they have no conflict of interest.

Data availability

No data was used for the research described in the article. request.

Declaration on the use of generative AI tools

During the preparation of this work, the authors used Chat GPT to improve language. After using this tool, the authors reviewed and edited the content as needed and take full responsibility for the content of the published article.

References

Aftab W, Hostettler R, De Freitas A, et al., 2019. Spatio-temporal gaussian process models for extended and group object tracking with irregular shapes. *IEEE Transactions on Vehicular Technology*, 68(3):2137-2151. https://doi.org/10.1109/TVT.2019.2891006

Baum M, Hanebeck UD, 2009. Random hypersurface models for extended object tracking. 2009 IEEE International Symposium on Signal Processing and Information Technology (ISSPIT), p.178-183.
https://doi.org/10.1109/ISSPIT.2009.5407526

Baum M, Hanebeck UD, 2014. Extended object tracking with random hypersurface models. *IEEE Transactions on Aerospace and Electronic Systems*, 50(1):149-159.
https://doi.org/10.1109/TAES.2013.120107

Cao X, Lan J, Li XR, 2021. Extension-deformation approach to extended object tracking. *IEEE Transactions on Aerospace and Electronic Systems*, 57(2):866-881.
https://doi.org/10.1109/TAES.2020.3034028

Cao X, Lan J, Liu W, et al., 2026. Maneuvering extended object tracking using extension-deformation approach with multiple reference extensions. *Signal Processing*, 244:110533.
https://doi.org/10.1016/j.sigpro.2026.110533

Eltoukhy M, Ahmad MO, Swamy MNS, 2020. An adaptive turn rate estimation for tracking a maneuvering target. *IEEE Access*, 8:94176-94189.
https://doi.org/10.1109/ACCESS.2020.2995672

Granstrom K, Baum M, Reuter S, 2016. Extended object tracking: Introduction, overview and applications. *arXiv preprint arXiv:160400970*, .

Han B, Huang H, Lei L, et al., 2019. An improved imm algorithm based on stsrckf for maneuvering target tracking. *IEEE Access*, 7:57795-57804.
https://doi.org/10.1109/ACCESS.2019.2912983

Kang M, Baek J, 2021. Sar image change detection via multiple-window processing with structural similarity. *Sensors*, 21(19):6645.

Koch JW, 2008. Bayesian approach to extended object and cluster tracking using random matrices. *IEEE Transactions on Aerospace and Electronic Systems*, 44(3):1042-1059.
https://doi.org/10.1109/TAES.2008.4655362

Lan J, Li XR, 2012. Tracking of extended object or target group using random matrix — part i: New model and approach. 2012 15th International Conference on Information Fusion, p.2177-2184.

Lan J, Li XR, Mu C, 2011. Best model augmentation for variable-structure multiple-model estimation. *IEEE Transactions on Aerospace and Electronic Systems*, 47(3):2008-2025.
https://doi.org/10.1109/TAES.2011.5937279

Lau TS, Tay WP, Veeravalli VV, 2019. A binning approach to quickest change detection with unknown post-change distribution. *IEEE Transactions on Signal Processing*, 67(3):609-621.
https://doi.org/10.1109/TSP.2018.2881666

Li Q, Song L, 2020. Axisymmetric extended target tracking using gaussian process. 2020 IEEE 3rd International Conference on Information Communication and Signal Processing (ICICSP), p.306-311.
https://doi.org/10.1109/ICICSP50920.2020.9232065

Li T, Liang H, Xiao B, et al., 2023. Finite mixture modeling in time series: A survey of bayesian filters and fusion approaches. *Information Fusion*, 98:101827.
https://doi.org/10.1016/j.inffus.2023.101827

Li T, Wang J, Li G, et al., 2025. From target tracking to targeting track — part iii: Stochastic process modeling and online learning. *IEEE Transactions on Signal Processing*, 73:5336-5347.
https://doi.org/10.1109/TSP.2025.3633496

Li XR, Bar-Shalom Y, 1996. Multiple-model estimation with variable structure. *IEEE Transactions on Automatic Control*, 41(4):478-493.
https://doi.org/10.1109/9.489270

Mannari P, Tharmarasa R, Kirubarajan T, 2024. Extended target tracking under multitarget tracking framework for convex polytope shapes. *Signal Processing*, 217:109321.
https://doi.org/10.1016/j.sigpro.2023.109321

Qian M, Chen W, Sun R, 2024. A maneuvering target tracking algorithm based on cooperative localization of multi-uavs with bearing-only measurements. *IEEE Transactions on Instrumentation and Measurement*, 73:1-11.
https://doi.org/10.1109/TIM.2024.3382741

Ricardo JA, Giacomossi L, Trentin JFS, et al., 2023. Cooperative threat engagement using drone swarms. *IEEE Access*, 11:9529-9546.
https://doi.org/10.1109/ACCESS.2023.3239817

Rong Li X, Jilkov V, 2005. Survey of maneuvering target tracking. part v. multiple-model methods. *IEEE Transactions on Aerospace and Electronic Systems*, 41(4):1255-1321.
https://doi.org/10.1109/TAES.2005.1561886

Shi H, Zhang X, Chen Y, 2022. Air defense mission planning of ship formation based on event network and monte carlo simulation. 2022 8th International Symposium on System Security, Safety, and Reliability (ISSSR), p.55-60.
https://doi.org/10.1109/ISSSR56778.2022.00016

Shi J, Cao X, Liu W, 2025. Adaptive tracking method for extended target based on gaussian processes. 2025 14th International Conference on Control, Automation and Information Sciences (ICCAIS), p.1-6.
https://doi.org/10.1109/ICCAIS67508.2025.11262084

Tuncer B, Orguner U, Özkan E, 2022. Multi-ellipsoidal extended target tracking with variational bayes inference. *IEEE Transactions on Signal Processing*, 70:3921-3934.
https://doi.org/10.1109/TSP.2022.3192617

Tuncer B, Özkan E, 2021. Random matrix based extended target tracking with orientation: A new model and inference. *IEEE Transactions on Signal Processing*, 69:1910-1923.
https://doi.org/10.1109/TSP.2021.3065136

Wahlström N, Özkan E, 2015. Extended target tracking using gaussian processes. *IEEE Transactions on Signal Processing*, 63(16):4165-4178.
https://doi.org/10.1109/TSP.2015.2424194

Wang L, Zhan R, 2024. Joint detection, tracking, and classification of multiple maneuvering star-convex extended targets. *IEEE Sensors Journal*, 24(4):5004-5024.
https://doi.org/10.1109/JSEN.2023.3347909

Wei Y, Lan J, Cheng Z, et al., 2025. Probabilistic flight envelope based joint tracking and classification using kinematic measurements. *IEEE Signal Processing Letters*, 32:2374-2378.

Xie L, Zou S, Xie Y, et al., 2021. Sequential (quickest) change detection: Classical results and new directions. *IEEE Journal on Selected Areas in Information Theory*, 2(2):494-514.
https://doi.org/10.1109/JSAIT.2021.3072962

Xu M, Yang C, Cao X, et al., 2024. Irregular extended target tracking with unknown measurement noise covariance. *Signal Processing*, 225:109600.
https://doi.org/10.1016/j.sigpro.2024.109600

Xue X, Wei D, Huang S, 2024. Cluster target tracking based on multi-sensor continuous-discrete pmbm filter. *Expert Systems with Applications*, 245:123121.
https://doi.org/10.1016/j.eswa.2023.123121

Yan H, Deng X, Bu S, et al., 2024. Research on maneuvering target tracking algorithm with adaptive turning rate based on dynamics model. 2024 6th International Conference on Electronic Engineering and Informatics (EEI), p.1243-1249.
https://doi.org/10.1109/EEI63073.2024.10696733

Yang D, Guo Y, Yin T, et al., 2023. Cost-effective gaussian processes based extended target tracking. *IEEE Transactions on Aerospace and Electronic Systems*, 59(6):8282-8296.
https://doi.org/10.1109/TAES.2023.3305320

Yang S, Baum M, 2019. Tracking the orientation and axes lengths of an elliptical extended object. *IEEE Transactions on Signal Processing*, 67(18):4720-4729.
https://doi.org/10.1109/TSP.2019.2929462

Yasin JN, Mohamed SAS, Haghbayan MH, et al., 2020. Energy-efficient formation morphing for collision avoidance in a swarm of drones. *IEEE Access*, 8:170681-170695.
https://doi.org/10.1109/ACCESS.2020.3024953

Zea A, Faion F, Baum M, et al., 2016. Level-set random hypersurface models for tracking nonconvex extended objects. *IEEE Transactions on Aerospace and Electronic Systems*, 52(6):2990-3007.
https://doi.org/10.1109/TAES.2016.130704

Zhang X, Yang Q, Lyu J, et al., 2024. Distributed variation parameter design for dynamic formation maneuvers with bearing constraints. *IEEE Transactions on Automation Science and Engineering*, 21(3):3664-3677.
https://doi.org/10.1109/TASE.2023.3283095

Zhang X, Liu H, Meng F, et al., 2023. Group target tracking via jointly optimizing group partition and association. *Automatica*, 153:111013.
https://doi.org/10.1016/j.automatica.2023.111013